Self-supervised High-fidelity and Re-renderable 3D Facial Reconstruction from a Single Image

Mingxin Yang, Jianwei Guo, Zhanglin Cheng, Xiaopeng Zhang, Dong-Ming Yan

Abstract—Reconstructing high-fidelity 3D facial texture from a single image is a challenging task since the lack of complete face information and the domain gap between the 3D face and 2D image. The most recent works tackle facial texture reconstruction problem by applying either generation-based or reconstruction-based methods. Although each method has its own advantage, none of them is capable of recovering a high-fidelity and re-renderable facial texture, where the term 're-renderable' demands the facial texture to be spatially complete and disentangled with environmental illumination. In this paper, we propose a novel self-supervised learning framework for reconstructing high-quality 3D faces from single-view images in-the-wild. Our main idea is to first utilize the prior generation module to produce a prior albedo, then leverage the detail refinement module to obtain detailed albedo. To further make facial textures disentangled with illumination, we present a novel detailed illumination representation which is reconstructed with the detailed albedo together. We also design several regularization loss functions on both the albedo side and illumination side to facilitate the disentanglement of these two factors. Finally, thanks to the differentiable rendering technique, our neural network can be efficiently trained in a self-supervised manner. Extensive experiments on challenging datasets demonstrate that our framework substantially outperforms state-of-the-art approaches in both qualitative and quantitative comparisons.

Index Terms—3D face modeling, self-supervised training, re-renderable, high-fidelity, facial texture reconstruction, illumination reconstruction

✦

1 INTRODUCTION

Reconstructing high-fidelity 3D human faces is a longstanding problem in computer vision and graphics communities. This task aims to estimate a realistic 3D facial representation, *i.e.,* estimating face geometry, appearance, expression, head pose, and scene lighting from the input source. Faithfully reconstructing 3D faces is a crucial prerequisite for many downstream applications, such as face editing [1], virtual avatar generation [2], [3] and side view face recognition [4].

Great attention is drawn into the most challenging problem of single image 3D face reconstruction because of the easy-to-get characteristic of RGB images and numerous available in-the-wild monocular facial images datasets. Considering that reconstruction from a single image is a highly ill-posed problem, a parametric model called *3D Morphable Model* (3DMM) [5] is developed as the prior model of a 3D human face that formulates the 3D face reconstruction into a parameter estimation problem. However, 3DMM largely limits the representation capability of the parametric model because it was constructed by applying linear subspace modelling techniques on a limited number of 3D face scans, thus leading to poor reconstruction fidelity [6], [7], [8]. Recently, many attempts have been conducted to tackle the detail lacking drawback of 3DMM by adding non-linearity into the parametric model, for example, replacing the linear 3DMM with a completely non-linear one [9], [10], [11] or complementing non-linearity upon the 3DMM coarse reconstruction [12], [13], [14], [15], [16], [17].

• *M. Yang, J. Guo, X. Zhang and D.M. Yan are with NLPR, Institute of Automation, Chinese Academy of Sciences, Beijing 100190, China., and School of Artificial Intelligence, University of Chinese Academy of Sciences, Beijing 100049, China.*
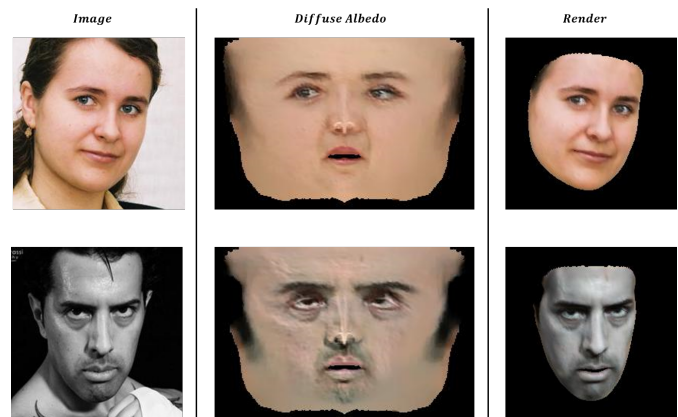• *Z. Cheng is with Shenzhen Institute of Advanced Technology, Chinese Academy of Sciences, China.*

Fig. 1: Our 3D facial texture reconstruction from single in-the-wild images. Left: input face images; middle: detailed albedo map generated by our neural network; right: re-rendered results using our recovered detailed albedo and detailed illumination.

In these methods, facial details are either represented in geometry by a displacement map (normal or depth map) or encoded into appearance by a detailed texture map (albedo map). In this study, we focus on the high-fidelity appearance reconstruction and apply a coarse-to-fine approach to generate textures that captures much facial details.

The methods for reconstructing high-fidelity facial textures can be roughly divided into two categories. The first category, which we call generation-based method, extends the basic idea of the parametric model and tries to learn a subspace of realistic facial textures [2], [7], [9], [18]. When estimating a new image, these approaches fit the closest texture in the subspace to the input. Accordingly, these appoaches could achieve high-quality

results even when the inputs are occluded or in extreme light condition. However, their requirement of realistic facial texture data for training leads to the problem that their generation results do not always conform to the input face because of the limited number of samples contained in the texture dataset, and extending such dataset needs laborious work. The other category of methods typically reconstructs the texture directly from the input image [12], [14]; therefore, we call it reconstruction-based method. The simplest approach is to directly leverage the unwrapped uv-texture from the image as the 3D facial texture [14]. Lin et al. [12] utilize the graph neural network to refine the 3DMM coarse texture to achieve high-fidelity results. Although their reconstruction corresponds to input image better, they share the same limitation, that is, the reconstruction quality is highly influenced by the input image, and noise-like occlusion and extreme environmental illumination will cause artifacts in the reconstructed texture.

Apart from the requirements of high-fidelity texture reconstruction, many applications (*e.g.,* virtual avatar generation) demand the texture to be re-renderable. Specifically, the reconstructed texture should be not only faithful to the input image, but also disentangled with illumination (which is referred as an albedo). However, the current generation-based and reconstruction-based methods can not solve the disentanglement of face albedo with illumination. The reasons are two-fold: (1) real facial textures are difficult to capture without illumination; and (2) the widely used spherical harmonics lighting model has a limited representational capacity. Lin et al. [12] represent the illumination by a three-band spherical harmonics which is not enough to capture spatially complex environmental illumination in the in-the-wild facial images. Gecer et al. [9] propose a dataset of high-fidelity facial textures; however, it has the drawback of illumination baked in, which still could not help illumination disentanglement.

To address the above-mentioned issues in the generation-based and reconstruction-based methods, we propose a new self-supervised learning algorithm that combines these two methods together to generate high-fidelity and re-renderable facial albedos. Our core idea is to first utilize a *prior albedo generation module* to first produce an albedo as a prior, and then add facial details on the prior albedo by using a *detail refinement module*. Specifically, we adopt a pre-trained inference network with a corresponding face parametric model to produce a prior albedo from the input image, similar to that in the generation-based approaches. Then, we transform the prior albedo to a high-fidelity one by using an image translation paradigm to preserve the detailed information in the input image. We present a novel detailed illumination representation and introduce a detailed illumination decoder in our coarse-to-fine framework to make the albedo disentangled with environmental illumination. Several regularization loss functions are designed in both the illumination side and albedo side to achieve a high-fidelity and re-renderable albedo. Finally, our pipeline can be efficiently trained in a self-supervised manner with the help of differentiable rendering [7].

In summary, our main contributions are as follows:

- We propose a new self-supervised neural network that possesses the advantages of both the generation-based and the reconstruction-based approaches to obtain a high-fidelity and re-renderable facial albedo. The self-supervised learning makes our approach generalize well among other unseen data.

- We devise a novel representation of detailed illumination by the extension of spherical harmonics to achieve a more accurate illumination estimation result, which contributes to the de-lightment of our albedo.
- We propose several regularization loss terms to ensure that the detailed albedo is similar to the prior coarse albedo while keeping realistic details of the input facial image.

2 RELATED WORK

2.1 Parametric Models for the Human Face

The 3D parametric model is a type of technique leveraging a limited number of parameters to control 3D facial attributes (i.e. geometry, appearance, and pose). The convenience to rig a 3D face model is beneficial to certain tasks such as facial animation, facial reconstruction, facial retargeting.

The seminal parametric model for the human face called 3D Morphable Model (3DMM) was first introduced by Blanz and Vetter [5]. This work applies a subspace modeling method on a collected 3D face scan dataset and produces low-dimensional representations for facial identity, expression and albedo. Since the 3DMM was proposed, many variants [19], [20], [21], [22], [23] have extended it to obtain better performance. Egger et al. [24] provide a comprehensive survey of 3DMM. Although these versions are different from the original 3DMM, they all utilize diverse variants of linear dimensional reduction approaches similar to that in [5], which limits their representation power of the low-dimensional controlling parameters. To solve this problem, parametric models with non-linearity are introduced. Non-linear 3DMM [10] utilizes CNN to replace linear encoder-decoder in the 3DMM and embeds it into a self-supervised 3D face reconstruction pipeline. Since the 3D ground truth is absent, this model takes the advantage of residue learning and splits the decoder into two branches: one for coarse reconstruction, which shares strong regularization; the other for capturing high-level details on the basis of four local patch reconstruction. Although this model expands the representation capacity of 3DMM, the local modeling scheme leads to stitching artifacts in the generated result. This model is also not a generative model like 3DMM (which assumes Gaussian distribution on the controlling parameters), therefore, it is not capable of directly generating new random samples from it.

Ganfit [9] utilizes a progressive GAN [18] to construct a generative parametric model, which collects a database of high-resolution human facial textures and trains the network on it. As mentioned in Section 1, the model has the drawback that the illumination is baked into the texture. Lattas et al. [2] extend Ganfit by post-processing (super-resolution, de-lighting and BRDF inference) the texture derived and achieves better results. The limitation of [2] is that the dataset captured does not contain sufficient samples on different ethnicities and may produce unfaithful results.

We choose the Basel Face Model (BFM) [25], which is also a variant of traditional linear 3DMM, as our parametric model in the prior generation module. Although the representation power of BFM is still limited, high-level detailed information can be complemented by our proposed detail refinement module. The albedo generated by the BFM is decoupled with light, and this provides us a good prior to guide detailed albedo reconstruction.

2.2 3D Face Reconstruction

Monocular face reconstruction. The methods for 3D face reconstruction can be roughly classified according to the input

sources, such as monocular face reconstruction, single RGBD face reconstruction and multi-RGBD face reconstruction, etc. In this study, we mostly consider the most challenging topic: monocular face reconstruction which learns a mapping from a single RGB image to a 3D face model. Given the lack of depth information in RGB images, 3DMM is always included as a proxy model in the face monocular face reconstruction pipeline. A variety of works [1], [6], [7], [8], [9], [14], [16], [26], [27], [28], [29], [30] utilize this paradigm to transform the reconstruction to a parameter estimation problem. These works can be further divided into two categories by the inferring approaches: fitting-based and learning-based methods. The former provides more accurate reconstruction results but consumes more time, while the latter leverages deep convolutional neural networks to estimate 3DMM parameters leading to a fast inference.

High-fidelity 3D face reconstruction. Although 3DMM is capable of reconstructing 3D face roughly, it lacks detailed information. Accordingly, the reconstruction results will lack certain characteristics such as wrinkles and pores. Recently, many methods were proposed for high-fidelity 3D reconstruction. The direct idea is to capture a dataset with high-quality 3D face ground-truth and train the inference deep network on the dataset [14], [31], [32], [33], [34] to achieve authentic reconstruction results. However, constructing such datasets requires expensive capture equipment (e.g., LED sphere) and leads to laborious work. Meanwhile, the data are mostly captured in a controlled environment and the network trained on it is hard to handle in-the-wild face images.

Richardson et al. [29], [30] utilize shape-from-shading to construct loss functions after conducting the 3DMM reconstruction to complement the details. Shape-from-shading attempts to infer geometry from an RGB image by solving the Irradiance Equation [35]. Since it is a highly ill-posed problem, regularization such as constant albedo or single point light source is often assumed, but this limits its representation power and leads to disability to recover all high-frequency details. With the development of CNNs and the introduction of differentiable rendering, a self-supervised paradigm with re-rendering loss is incorporated into the facial detail reconstruction [10], [11], [12], [13], [15], [16]. These works add a regression network to complement detail information upon the 3DMM coarse reconstruction. However, the coarse model and detail model are often trained separately. These approaches are trained in in-the-wild image datasets and resolve the drawbacks of supervised approaches. Wu et al. [36] leverage the symmetry in the human face and directly regress the depth maps; however, it is unable to reconstruct a complete face model and produce artifacts when encountering extreme inputs (e.g., images with non-frontal faces). Other than the above-mentioned 3D face reconstruction methods, another branch of work focuses on human portrait video synthesis. Many of these methods [37], [38], [39] still utilize the 3DMM as an intermediate representation and generate high-fidelity details upon it. However, these works do not produce any detailed 3D face model;hence, their reconstruction results can not be directly utilized by graphic renderers.

Representation of facial details. 3D facial detail information can be modeled in either geometric space as displacements or normal [10], [11], [14] or in appearance space as texture or albedo [9], [12], [40]. Considering the representation space, details can be represented as maps in uv-space, or maps in frontal-face space, or vertex attributes on a 3D face mesh. The methods of [10], [14] represent facial detail in uv-space. Chen et al. [14] unwrap partial image texture from image and regress a detailed

displacement map from it; Tran et al. [10] directly generate a uv representation of texture and geometry from the input image. Lin et al. [12] utilize graph convolutional network (GCN) and model texture as three-channel vertex attributes on a 3D face mesh to obtain competitive results. Wu et al. [36] take advantage of the symmetry characteristic of human faces and represent the depth, albedo and illumination maps in the frontal-face space. Although applying GCN on mesh could produce convincing results, we argue that uv-representation is still a valid representation for detail reconstruction because the proper face parameterization keeps most of the face topology and can be easily processed by 2D CNN. In this work, we present a monocular high-fidelity 3D face reconstruction approach and represent the detail information by a detailed texture map in the uv-space.

3D face reconstruction with other inputs. Some studies utilize more input data than a single image. Luo et al. [41] take a single depth image as the input and estimate the coarse geometry from it. Wang et al. [42] construct a dataset with uncalibrated sparse photometric stereo images with a geometric ground-truth and train a convolutional neural network to infer high-fidelity geometry.

2.3 Image Formation Modeling

Image formation is the process that maps the 3D model with an environmental condition to a 2D image space. The core in the process is the reflectance models that include illumination modeling and interaction pattern between light and the model surface. In 3D face modeling, three-band RGB spherical harmonic lighting representation [43] and Lambertian surface are often considered the default settings [6], [10], [12]. Spherical harmonics is a set of orthonormal basis defined on a sphere that is analogous to Fourier basis in the Euclidean space, and it can be a proper approximation to illumination in the natural lighting. Lambertian surface assumes that the surface irradiance is irrelevant to the observer's position and only depends on the incident light direction. Although these two assumptions provide proper approximation, they neglect other reflection effects (such as specular reflection) in the real scenario and limit the capability to capture complete illumination when encountered with complex environmental light, which is harmful to recover detailed face albedo. This observation motivates us to also refine the reflectance models in our method. Therefore, we propose to retain the Lambertian assumption and attribute all the complex reflectance into our detailed illumination map which is an extension of 3-band spherical harmonics.

2.4 Differentiable Renderer

Differentiable rendering is a key module in our self-supervised pipeline whose goal is to render a 3D model with corresponding attributes to a 2D image in a fully differentiable way. To be incorporated into neural networks, the core idea is to provide the gradient when doing backward passing. With regard to facial reconstruction, recent studies such as [44], [45], [46] and [47] can be taken into our framework. Zhu et al. [45] and Liu et al. [46] soften the rasterizing process and are fully differentiable even in forward passing while others only calculate the pseudo-gradients during the backward passing. We utilize [44] for our differentiable rendering for efficient inference.

3 OVERVIEW

Given a single facial image, our goal is to reconstruct a 3D human face, with the emphasis on generating a high-fidelity
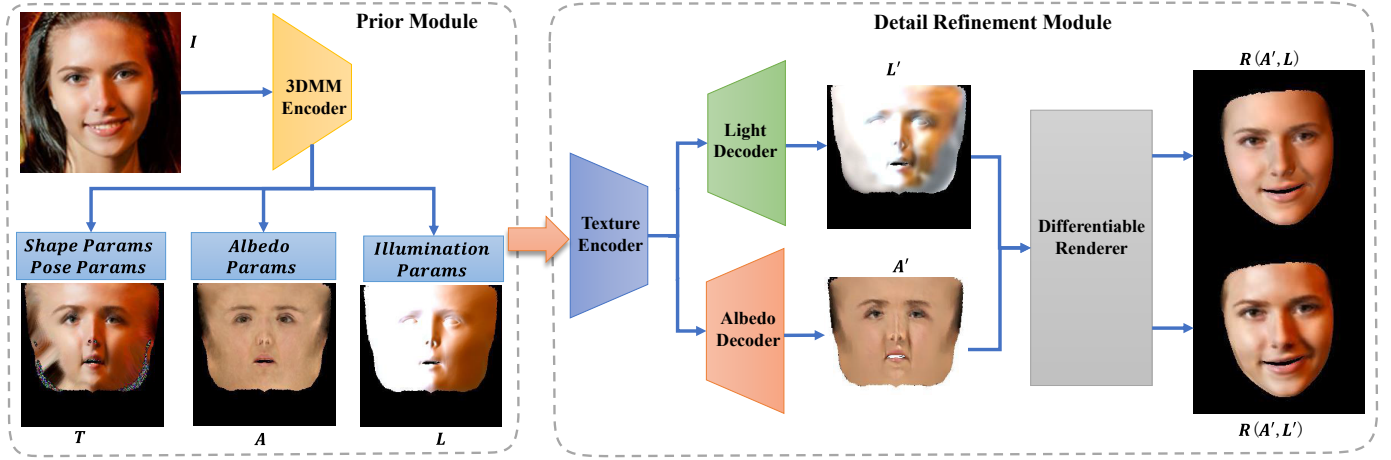
Fig. 2: **Network architecture for 3D face reconstruction:** The left part shows our prior module that takes a 3DMM as proxy model and generates unwrapped facial texture map (T), prior albedo map (A) and prior illumination (L). Our prior module includes a pre-trained 3DMM encoder to regress 3DMM parameters from input image (I) and a fixed 3DMM linear decoder to generate corresponding attributes of the 3D face. The unwrapped facial texture map and prior albedo map are then fed into our detail refinement module (right part in the figure) to generate the detailed albedo ($A^{'}$) and detailed illumination ($L^{'}$). The detail refinement module contains one texture encoder with a light decoder and an albedo decoder. After getting the detailed illumination map and the detailed albedo map, they are sent to a differentiable renderer with other 3D face attributes to obtain re-rendered images ($R(A^{'}, L^{'}), R(A^{'}, L)$) for self-supervision.

and re-renderable facial texture that is complete, detailed and disentangled with illumination.

To this end, we propose to first generate a prior albedo by a prior albedo generation module and enhance it with the facial texture unwrapped from the image by a detail refinement module, (Fig. 2). A high-quality albedo dataset is needed to train the parametric model adopted in prior albedo generation module. Although Gecer et al. [9] collect a dataset of facial textures, the samples in it are not re-renderable (thus cannot be referred as albedo) because of the baked-in illumination. To the best of our knowledge, no existing large open-source facial albedo dataset is available to date. Therefore, we choose a traditional linear 3DMM [25] as our parametric model because a 3DMM albedo excludes the illumination out. The other parametric models like [9] can also be directly applied in our pipeline.

In our framework, the input facial image is first fed into the 3DMM encoder to produce 3DMM parameters (including identity, expression, and albedo), pose parameters and illumination parameters. Then, these regressed 3DMM parameters are passed to a fixed 3DMM decoder to acquire the prior albedo, 3DMM shape, camera pose matrix and coarse illumination. Next, we obtain the facial texture by unwrapping the input image according to the projected 3DMM shape. The unwrapped facial texture map and prior albedo map are fed into the detail refinement module, which is composed of a modified version of image-to-image translation network, to generate a detailed albedo map and a detailed illumination map. Finally, the detailed albedo and the detailed illumination combined with the 3DMM shape projected in camera space are rendered to the image space by a differentiable renderer.

4 METHODOLOGY

4.1 Prior Albedo Generation Module

Our prior albedo generation module takes a 3DMM as proxy model and uses a convolutional neural network to estimate the parameters of facial geometry, albedo, pose and illumination. We

adopt the state-of-the-art 3DMM coefficient regressor [6] for the purpose. After the input image in fed to the network, a 257–dimensional parameter vector is regressed of which 80 is for shape, 64 for expression, 80 for albedo, 27 for illumination and 6 for camera pose. A textured 3D face model can be recovered by these parameters with a 3DMM decoder. As demonstrated in [5], the color and position of vertices can be represented as follows:

$$A = \overline{A} + F_A \Theta_A, \tag{1}$$

$$S = \overline{S} + F_I \Theta_I + F_E \Theta_E, \tag{2}$$

where $A \in \mathbb{R}^{3 \times N}, S \in \mathbb{R}^{3 \times N}$ represent the albedo and shape of the recovered 3D face with N vertices. $\overline{A} \in \mathbb{R}^{3 \times N}$ and $\overline{S} \in \mathbb{R}^{3 \times N}$ symbolize the mean albedo and mean shape of the 3DMM. F_E, F_I and F_A are the fixed basis of expression, identity and appearance in the 3DMM model, while Θ_E, Θ_I and Θ_A represent the expression, identity and albedo coefficients, respectively. These variables are incorporated into the decoder by a direct matrix multiplication.

In illumination reconstruction, we assume a Lambertian surface for the face material and utilize 3-band RGB spherical harmonics to represent the environmental illumination. The reflection of a vertex s_i with vertex normal n_i and albedo a_i can be computed as follows:

$$T_{s_i}(n_i, a_i, \Theta_L) = a_i \times \sum_{b=1}^{27} \Theta_L^b \Phi_b(n_i), \tag{3}$$

where Θ_L represents the illumination parameters and $\Phi_b \in \mathbb{R}^3 \rightarrow \mathbb{R}$ represents the spherical harmonics function.

On the basis of the above reconstruction, we can derive the prior albedo by 3DMM albedo decoding and generate an image texture by sampling the corresponding projection pixels with 3DMM shape and pose parameters. After these two textures are obtained, they are projected onto 2D uv-space to accommodate with 2D CNN structure of detail refinement module. However, two problems are introduced in the image texture sampling procedure.

First, the non-frontal face and occlusion problem in the facial images may cause incompleteness in the unwrapped texture. Second, the inaccurate regression of pose and shape parameters in many cases may also cause the image texture to generate artifacts, especially in the edge parts. Our detail refinement module introduced in the following section can resolve these two problems.

4.2 Detail Refinement Module

Our detail refinement module adopts an image-to-image translation network in the uv-space where the input of the network includes two maps: a prior albedo map and a partial facial image texture. We first pad the unseen parts with Gaussian noises as being carried out in [40] because filling the 'holes' in the unwrapped image texture is one of the goals of our detail refinement module. Then, these two maps are concatenated and fed into the refinement network. The detail refinement network also produces two outputs, the detailed albedo map and the detailed illumination map. The detailed albedo map includes information about basic details in human faces, such as facial wrinkles, pores and etc. Meanwhile the detailed illumination map attempts to model spatially-complex environmental illumination that can not be captured in a previous coarse reconstruction. Next, we elaborate on each part of the module and explain the specifically-devised loss functions.

4.2.1 Illumination Disentanglement

Illumination regularization. With respect to the illumination modeling, directly utilizing the coarse illumination in the prior generation module does not fully capture the complex illumination for the in-the-wild images. This situation will lead to the leakage of light information to the albedo which makes it not rerenderable. Therefore, a detailed representation for illumination is needed.

Given that our framework is trained in a self-supervised way, disentangling the illumination with albedo is not trivial. We take advantage of the coarse illumination spherical harmonics generated by the prior module and develop our illumination representation from it. We introduce a novel representation in the uv-space called spherical harmonics map which models a spherical harmonics illumination for every vertex in the face model. With the illumination map, we could not only model complex illumination in facial images, but also disentangle light by minimizing the distance with coarse spherical harmonics, which is named by illumination regularization loss. In particular, we represent the detailed illumination map $L_{detail} \in \mathbb{R}^{(B,27,H,W)}$ in the uv-space and directly regress it from the detail refinement module. Then, we regularize local illumination by devising a mean square error (MSE) loss to penalize detail and coarse illumination differences. The MSE loss is expressed as follows:

$$L_{reg-illu} = ||M_{uv} * (L_{detail} - L_{coarse})||^2, \quad (4)$$

where $L_{coarse} \in \mathbb{R}^{(B,27,H,W)}$ is the coarse SH-illumination vector expanding to uv map size, and $M_{uv} \in \mathbb{R}^{(B,1,H,W)}$ stands for the uv-mask which represents the projected region of 3D face model in the uv-space.

Cross perceptual loss. Despite utilizing the illumination regularization loss mentioned above, we find in our experiments that a small amount of facial internal characteristics (such as wrinkles and beard) are mistakenly included in the illumination map, which means that albedo and illumination are not completely disentangled, leading to the loss of details in our detailed albedo map. Given that the attributes, such as wrinkles and beard are

Fig. 3: **Motivation of the cross perceptual loss.** From left to right are image of identity A, image of identity B, the rendered image constructed by detailed albedo of A in combination with detailed illumination of B without cross perceptual loss, the rendered image constructed by detailed albedo of A in combination with detailed illumination of B with cross perceptual loss

individual specific, we propose to utilize a cross-identity perceptual loss to conduct the further disentanglement. The motivation is stated below. We assume that the re-rendered image that combines person A's detailed illumination map and person B's detailed albedo map should have the same identity with person B in that the correctly-disentangled detailed illumination map would only include environmental illumination information in it. However, if the detailed illumination map is not entirely disentangled, which refers to including the facial attribute specific to person A, then it may change the identity of the rendered image. These two samples can be seen from Fig. 3. Owing to this observation, we utilize an illumination-irrelevant facial recognition network [48] to distinguish whether the two images are of the same identity. The cross perceptual loss is represented as follows:

$$L_{cross-percp} = 1- < ArcFace(I_r), ArcFace(I_{gt}) >, \quad (5)$$

where $ArcFace$ stands for the perceptual net, I_r represents the rendered image with detailed illumination map A and detailed albedo map B, and I_{gt} means the ground-truth facial image of B. We adopt the cosine distance as the measurement of the similarity between two normalized facial feature vectors.

We sum these two losses together with corresponding weights as our final illumination disentanglement loss:

$$L_{id} = \lambda_{id1} * L_{reg-illu} + \lambda_{id2} * L_{cross-percp}. \quad (6)$$

4.2.2 Albedo Regularization

We utilize prior albedo and the intrinsic characteristics of albedo map to construct several regularization losses for obtaining a complete and re-renderable albedo from the input image. Here, we propose three losses : the symmetry loss, albedo smooth loss, and conditional GAN losses.

(1) Symmetry loss: We propose a symmetry loss on the detailed albedo map. Given that human facial albedos are mostly symmetrical (especially when decoupled with light), we use this loss to regularize an unseen texture problem induced by the non-frontal face in the input image. Another advantage of the albedo symmetry loss is that it ensures robust albedo reconstruction in uneven scene illumination. The symmetry loss is expressed as follows:

$$L_{symm} = ||M_{uv} * (A_{detail} - \hat{A_{detail}})||^2, \quad (7)$$

where $\hat{A_{detail}}$ is the detailed albedo map flipped along the y-axis.

(2) Albedo smooth loss: We propose a smooth loss to regularize the detailed albedo map. We expect the detailed albedo map inherit this feature because the generated prior albedo is decoupled with illumination. We utilize local weighted smooth loss on the

detailed albedo map to achieve this goal. In computing the local weights, we assume the detailed albedo map shares the same smoothness with the prior albedo map. Therefore, we leverage the local difference between pixels in the prior albedo map to compute the smoothness weights of the detailed albedo map. The albedo smooth loss is defined as:

$$L_{smooth} = \sum_i \sum_{j \in N(i)} \omega_{i,j} ||A_{detail}(i) - A_{detail}(j)||^2, \quad (8)$$

$$\omega_{i,j} = exp(-\alpha * ||A_{prior}(i) - A_{prior}(j)||^2), \quad (9)$$

where A_{detail} and A_{prior} represent the detailed albedo map and the prior albedo map respectively, $N(i)$ indicates the neighbors of texel (pixel in uv-space) $p(i)$, $\omega_{i,j}$ represents the similarity of two texels, which is measured by a decreasing function of corresponding texels' difference in the prior albedo map. α is a super-parameter which we here choose 80 empirically [15]. In the above equation, our albedo smooth loss penalizes more to those texels whose neighborhood difference shares less similarity between the detailed albedo map and the prior albedo map.

(3) GAN loss: Our devised GAN loss includes an L_1 distance loss and an adversarial loss [49] to force the detailed albedo to share the same distribution as prior albedo map. The L_1 distance loss can be written as:

$$L_{L1} = |M_{uv} * (A_{detail} - A_{prior})|. \quad (10)$$

We then define the adversarial loss as:

$$L_{GAN_D} = E_{G(z) \in A_{detail}} log(1 - D(G(z))) + \quad (11)$$
$$E_{x \in A_{prior}} log D(x),$$
$$L_{GAN_G} = E_{G(z) \in A_{detail}} log(D(G(z))). \quad (12)$$

where D symbolizes the discriminator to judge whether the generated albedo map falls on the support set of the prior albedo map distribution. $G(z)$ represents the detailed albedo map generator which means the whole framework introduced above.

Our albedo regularization loss is then computed by combining above four loss terms with proper weights:

$$L_{ar} = \lambda_{ar1} * L_{symm} + \lambda_{ar2} * L_{smooth} + \lambda_{ar3} * L_{L1} + \lambda_{ar4} * L_{GAN_G} \quad (13)$$

4.2.3 Detail Preservation

Besides above regularization losses, we also utilize basic reconstruction losses to facilitate high-fidelity reconstruction. These losses are all applied on the image space; thus a face mask is required for concentrating penalization of the differences on face regions in the images. We adopt the face parsing approach [50] to generate face masks before training. Coarse reconstruction may not be well-suited to image mask because of the inaccurate estimation of 3DMM and camera pose. Hence, we generate our final face mask by multiplying a pre-generated mask with projected face mask. The final face mask can be computed as:

$$M_{face} = M_{parsing} * M_{proj}. \quad (14)$$

After face masks are obtained, we propose two reconstruction losses applied in the mask regions, which contain image gradient loss and image loss.

(1) Image gradient loss: We now propose an image gradient loss to encourage the similarity between the re-rendered facial image gradient and the ground-truth facial image gradient for reconstructing facial details as authentic as possible. This loss is designed according to the assumption that the detail information can be mostly captured by image gradient. We define such gradient loss function as:

$$L_{grad} = \sum ||M_{face} * (Grad(I_r) - Grad(I_{gt}))||^2, \quad (15)$$

where M_{face} is the pre-extracted face mask, I_r and I_{gt} are the rendered image and the input facial image, respectively; and $Grad$ represents the gradient operator. Specifically, we first calculate two directional gradients along the x-axis and y-axis, then compare them with corresponding ground-truth gradient maps. Finally, we obtain the summation.

Given that gradients are mostly relevant to facial inherent details such as wrinkles and pores, we should model them in the detailed facial albedo map rather than in the detailed illumination map. To achieve this goal, we add another layer to render a facial image with coarsely-reconstructed illumination and the detailed albedo map to obtain albedo-detail-only rendered image. We then apply our gradient loss on this image instead of the image that is rendered by using the detailed albedo and the detailed illumination to facilitate the detailed albedo map containing more facial detailed information.

(2) Image loss: We also adopt image loss to penalize pixel difference between the rendered image and the input facial image, which can be expressed as follows:

$$L_{img} = \sum ||M_{face} * (I_r - I_{gt})||^2. \quad (16)$$

We combine these two losses together to obtain our detail preservation loss:

$$L_{dp} = \lambda_{dp1} * L_{grad} + \lambda_{dp2} * L_{img}. \quad (17)$$

4.3 Network Architecture and Training Details

We train our neural network on a public dataset CelebA [51] which is a large-scale facial attribute dataset that has more than 200K facial images collected from the internet. We separate the dataset into disjoint training data (85%) and testing data (15%). We pre-process the images by first generating 68-landmarks [52] before feeding them into our detail generation network. Then, we utilize the generated landmarks to crop and scale the images to keep the human faces staying in the center of the images and resize them to 224×224. After pre-processing, these images are fed into our pre-trained prior albedo generation module. In this work, a 3DMM parameter regressing network and a fixed 3DMM decoder (Basel Face Model decoder [25]) are utilized to obtain the prior albedo and other attributes (geometry, camera and illumination). The camera parameters and 3DMM shape are leveraged to unwrap the texture from the input image. Next, the unwrapped texture and prior albedo (in uv-space) are concatenated and fed into the detail reconstruction network to acquire detailed albedo maps and detailed illumination maps. Given that the vertex number of the 3DMM we adopted is 35709, we adopt the resolution of uv maps as 256×256 because the effective parameterization part of the uv map could contain all the vertices in the model.

We adopt the ResNet-50 [53] as the backbone network of our prior albedo generation module and pre-train it on 300W-LP [54] following the state-of-art 3DMM reconstruction work [6]. 300W-LP is a dataset that contains 122,450 facial images with a variety of head poses generated from the original 300W dataset by face profiling techniques. Similar to the training process in [6], we train the network self-supervisedly with pixel-level, landmark-level and

perceptual level discrepancy in combination with the parameter regularization loss.

In the detail reconstruction network, we adopt the basic pix2pix network [49] as our backbone and abandon the skip-connection because it may cause the output to inherit the noise from the un-wrapped image texture. We also extend pix2pix with two decoders, one for detailed albedo generation and the other for detailed illumination modeling. Tables 1 and 2 summarize the network architectures of our encoder and decoder, respectively. The light decoder and albedo decoder share the same structure but with different output layers, where the light decoder outputs a 27-channel map while the albedo decoder outputs a 3-channel one. Finally, We use the face mesh renderer [44] for differentiable rendering. We combine the loss functions mentioned above to train our network, which is expressed as follows:

$$L_{total} = L_{id} + L_{ar} + L_{dp}. \tag{18}$$

The coefficients in those loss functions are chosen as λ_{id1}, λ_{id2}, λ_{ar1}, λ_{ar2}, λ_{ar3}, λ_{ar4}, λ_{dp1}, λ_{dp2} : 1.0, 0.5, 5.0, 5.0, 1, 1.0, 0.001, 1.0, 5.0, where λ_{ar3} is set as 0.0 after first epoch training.

TABLE 1: Detailed architecture of our encoder. $Conv(c_{in}, c_{out}, k, s, p)$ refers to a convolution with c_{in} input channels, c_{out} output channels, kernel size k, stride s and padding p. InsNorm stands for instance normalization, and we use the LeakyReLU for activation.

Encoder	Output Shape
Conv(6,64,3,1,1), InsNorm, LeakyReLU	256
Conv(64,64,4,2,1), InsNorm, LeakyReLU	128
Conv(64,128,4,2,1), InsNorm, LeakyReLU	64
Conv(128,256,4,2,1), InsNorm, LeakyReLU	32
Conv(256,512,4,2,1), InsNorm, LeakyReLU	16

TABLE 2: Architecture of our decoders, where we use Transconv for transpose convolution and InsNorm for instance normalization. In the last layer a Conv operator is used to alleviate checkerboard artifacts caused by transpose convolution. The letter 'n' in the last Conv stands for the output channel, where we take a three-channel for albedo decoder and 27-channel for illumination decoder.

Decoder	Output Shape
TransConv(512,256,4,2,1), InsNorm, ReLU	32
TransConv(256,128,4,2,1), InsNorm, ReLU	64
TransConv(128,64,4,2,1), InsNorm, ReLU	128
TransConv(64,64,4,2,1), InsNorm, ReLU	256
Conv(64,n,3,1,1)	256

We trained our entire network end-to-end for 10 epochs using the Adam optimizer [55]. The initial learning rate was set to 10^{-4} and reduced with attenuation coefficient of 0.98 every 1 epochs until we reached 10^{-5} to avoid overfitting. The batch size was 16 and the momentum was 0.9. The training task was completed in 2 days on a workstation equipped with one Nvidia RTX-2080 TI GPU. Once trained, our network can process approximately 30 images per second in the inference stage.

5 EXPERIMENTAL RESULTS

We start with several experiments through visually inspecting our results on two well-known datasets to demonstrate the effectiveness of our proposed method. Then, we evaluate our algorithm
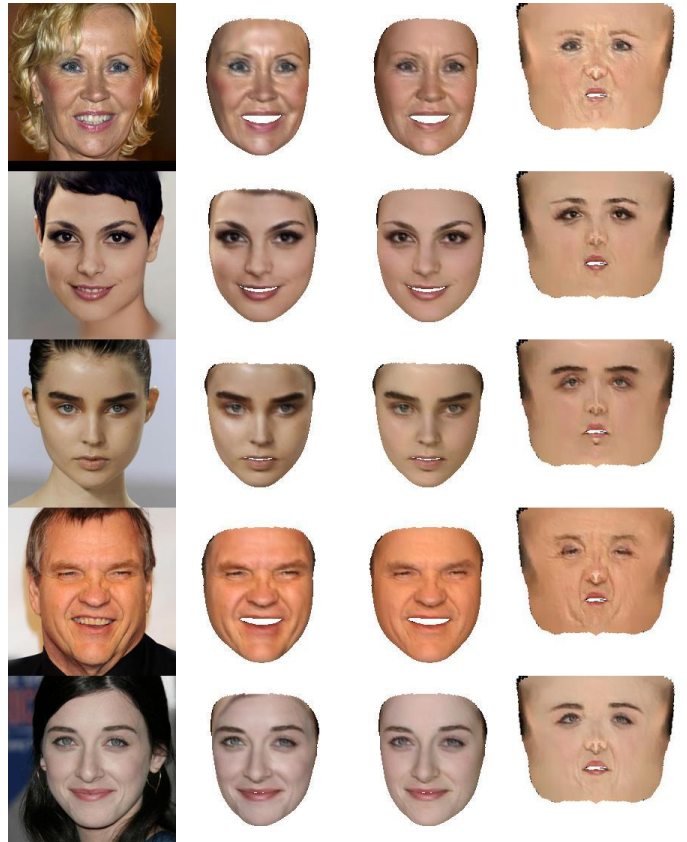

Fig. 4: **Our qualitative reconstruction results on CelebAHQ.** The first column is input images, the second and third columns show the reconstruction results generated by our detailed albedo combined with detailed illumination and coarse illumination respectively. The last column illustrates the detailed albedo in the uv-space.

qualitatively and quantitatively by performing a complete comparison with current state-of-the-art approaches. We further conduct ablation studies to provide a comprehensive evaluation of the individual components of our neural network.

5.1 Evaluation

Performance on CelebAHQ dataset. We first analyze the capability of our method by using the CelebAHQ database [56], which includes 30k 1024×1024 facial images generated by applying super-resolution algorithm to a subset of CelebA images. Given that the images in CelebAHQ contain more details than the original CelebA data, we test our neural network on this dataset to demonstrate if our proposed approach could capture details on high-definition images and achieve high-quality reconstructed albedo. Note that our neural network is only trained on the original CelebA dataset.

Fig. 4 qualitatively shows our reconstruction results on several images randomly selected from CelebAHQ. We leverage the figure to see whether our network could generate high-fidelity and re-renderable facial albedo. Our proposed approach successfully keeps the facial details in the reconstructed detailed albedo map, and there exists no reflection effects other than diffuse reflection in the albedo map or rendered results with coarse illumination. This phenomenon verifies that most of the environment illumination are

Fig. 5: **3D face reconstruction on two random FaceWareHouse(FWH) [20] samples.** From top to bottom are input images, coarse reconstructed albedo overlay results, reconstructed detailed albedo overlay results, detailed illumination rendered to image space, detailed albedo combined with detailed illumination overlay results.

explained by the detailed illumination, which leads to a clean diffuse facial albedo. In addition, our proposed albedo regularization loss ensure that the detailed albedo map also exhibits smoothness and completeness which are beneficial to re-render applications. The detailed albedo generated by our network can be directly sent into a renderer with Lambertian reflector to achieve high-fidelity re-rendered results owing to these two characteristics.

Performance on FaceWareHouse dataset. We use the FaceWareHouse (FWH) [20] database to test the network trained on CelebA dataset and demonstrate the generalization ability and robustness of our model. FWH includes 150 identities and each identity is captured with 20 specified expressions in a fixed environment. This database not only contains many challenging cases, such as high-frequency facial wrinkles generated by numerous expressions, but also includes the samples from the same identity in a fixed environment which leads to a rather stationary illumination condition. The second feature provides us a qualitative way to judge whether the environmental illumination is entirely explained by our proposed detailed illumination by inspecting if the detailed illumination maps of the same identity are close to each other.

Fig. 5 shows the reconstruction results of two randomly selected identities. In the fifth row, the high-fidelity reconstruction results demonstrate that our model has good generalization ability and is robust enough to capture facial details in another dataset. The second and third rows show the prior albedo and detailed albedo, respectively. The detailed albdeo shares strong appearance similarity to the prior coarse albedo while still preserving more details. The similarity in the whole appearance proves that the prior albedo generated by 3DMM serves as an effective guidance in the detailed albedo reconstruction. The fourth row illustrates the detailed illumination that is rendered to the image space. The rendered detailed illumination images from the same identity have a similar appearance, which verifies the detailed illumination in
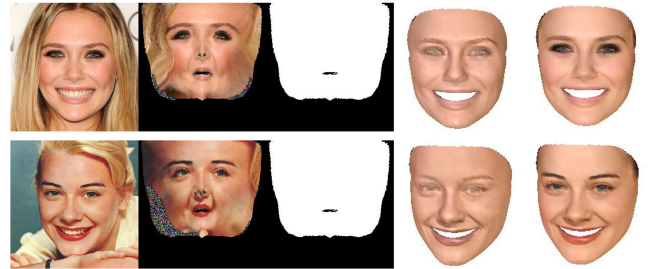

Fig. 6: **Evaluation of prior albedo and detail refinement module.** The first three columns are input images, unwrapped image textures, and white facial albedo, which replaces the coarse albedo. The right two columns show the output rendered images by using white albedo and original coarse albedo. The figure verifies the capability of our model to transfer as much details from the input texture.

our model correctly captures the environmental light.

Evaluation of prior albedo and detail refinement module. Given that the detail refinement module in our framework takes two inputs, namely the prior albedo generated by 3DMM and the unwrapped texture from the input image, we are interested in exploring what these two inputs are responsible for in the detail refinement module. Accordinglym we conduct an experiment by substituting the input prior 3DMM albedo by a white map (so it includes no prior information) to evaluate the effect of the inputs. Fig. 6 shows the experimental results, where the rendered image with white map absorbs most details in the input but loses the appearance consistency with the original image. This phenomenon indicates that our detail refinement module takes these two inputs independently, where the prior albedo guides entire appearance
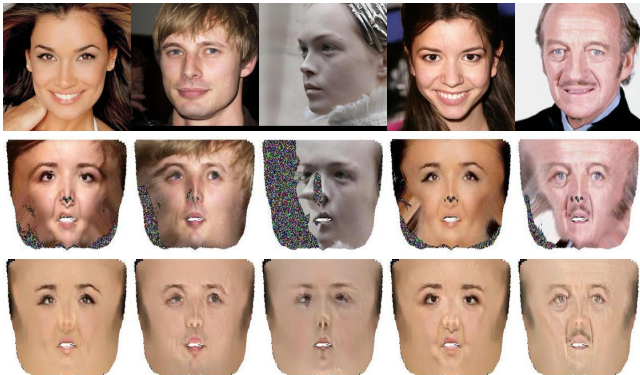
Fig. 7: **Effectiveness of eliminating artifacts in unwrapped image texture.** From top to bottom are original input facial images, the unwrapped textures from input images and detailed albedos constructed by our method.

generation and the unwrapped texture is responsible for the detail supplement.

Texture artifact removal. We now evaluate the capability of our detail refinement module in dealing with the textures containing artifacts. The two main artifacts that exist in facial images are show in the second row of Fig. 7. First, the non-frontal face images would lead to incompleteness in the unwrapped image texture. Second, the geometry parameters (including camera pose and shape parameters) regressed from the coarse reconstruction step are not accurate in many cases, which would result in severe stripe-like artifacts in the unwrapped texture, especially in the boundaries of human face. Our detail refinement module can remove these two kinds of artifacts and produce a smooth, complete and high-fidelity albedo (Fig. 7). This phenomenon is mainly due to the introduction of prior albedo and our designed albedo regularization loss, which endow the final reconstructed albedo with completeness and smoothness.

5.2 Qualitative Comparison

For qualitative comparison, we first compare the reconstruction results of our approach against recent state-of-the-art deep-learning-based texture reconstruction methods [6], [7], [9], [12] on some representative data samples. Then, we focus on the qualitative evaluation in extreme illumination condition and compare our reconstructed albedo with advanced facial texture generation method [9].

Qualitative comparison on MOFA data. Fig. 8 compares the reconstruction results on a subset of MOFA test dataset [8]. Lin et al. [12] aim to reconstruct high-fidelity facial texture from a single image self-supervisedly. They achieve this goal by also first utilizing the coarse albedo generated from 3DMM then fine-tuning it by a face feature extracted from the image according to a pre-trained face recognition network (FaceNet [57]). They leverage a GCN as and the fine-tune module and represent the albedo on a mesh level (per-vertex albedo). Although looks similar, the target of our method is not exactly the same as theirs because we expect our reconstructed albedo to exhibit not only high-fidelity but also smooth, complete and decoupled from environmental illumination. Accordingly, our reconstructed albedo can be directly re-rendered by any renderer with a Lambertian reflector. Therefore, the third and fourth rows illustrate that, our albedo renderers capture more

internal facial details than [12] while leaving the complex environmental illumination and other reflection effects (such as specular reflection) aside from diffuse reflection to our detailed illumination map. Considering the main differences in implementation, our network has an additional illumination modeling module that accounts for the complex environmental illumination and we get rid of the pre-trained face feature extraction network used in [12]. It is also worth noticing that the prior albedo generation module in our framework can be directly replaced by any generation model which leads to a strong extendibility of our work.

As a generation-based model, Gecer et al. [9] capture 10,000 high-resolution human facial textures in the uv-space and train a progressive growing GAN to model the distribution human face texture. They leverage this progressive GAN as the generative model and utilize fitting-based paradigm to estimate the parameters in latent space. The fifth row in Fig. 8 show that the reconstruction results lose much fidelity from the original input face and are not alike in appearance. The phenomenon is especially severe for in-the-wild situations. This phenomenon could be attribute to the limited number of captured data that cannot span all of the face texture space. By constrat, our model utilizes a less expressive generative model (Basel Face Model 2009) but achieves better reconstruction fidelity.

Deng et al. [6] and Genova et al. [7] are the two representative 3DMM-based facial reconstruction methods that are also trained in the self-supervised way on in-the-wild facial image datasets. The sixth and seventh rows show the reconstruction results of these methods. The 3DMM-based reconstruction approach has the advantages of obtaining smoothness and completeness but loses most of the details in the face, which produces much less convincing results than our approach.

Qualitative comparison on extreme illumination data Facial images under extreme illumination condition, including uneven lighting or shadow, are commonly encountered in real-world applications. Due to the loss of information and low quality representation of illumination (three-band Spherical Harmonics), reconstructing high-fidelity 3D face under such circumstances is still challenging thus reconstruction-based methods always fail to reconstruct complete face albedos. Meanwhile, a generation-based approach can deal with extreme lighting because they map the facial texture space to a latent space with a support set. Our proposed model merging these two methods together should also have the capability to reconstruct convincing face albedos from the facial images under extreme illumination. In Fig. 9, we compare our reconstruction results in extreme lighting to a generation-based method, Ganfit [9]. The second and third columns show that our albedo decouples the complex environmental illumination and outperforms [9] by preserving more facial details from the input face. This phenomenon is because of the cooperation between the prior albedo generation module with the detail refinement module of our framework. The former module is responsible for generating the guided albedo and the latter can complement details upon it. As a result, our method not only inherits the advantage of generation-based methods which maintain the diffuse texture smooth in the whole but also has the ability to preserve the details as in a reconstruction-based method. We outperform Ganfit and achieve more convincing results. The fourth column shows re-illuminated results according to our reconstructed albedo, where we apply different illumination conditions to the reconstructed albedo and render it to images where the illumination is randomly selected from a face illumination prior database [58]. The re-
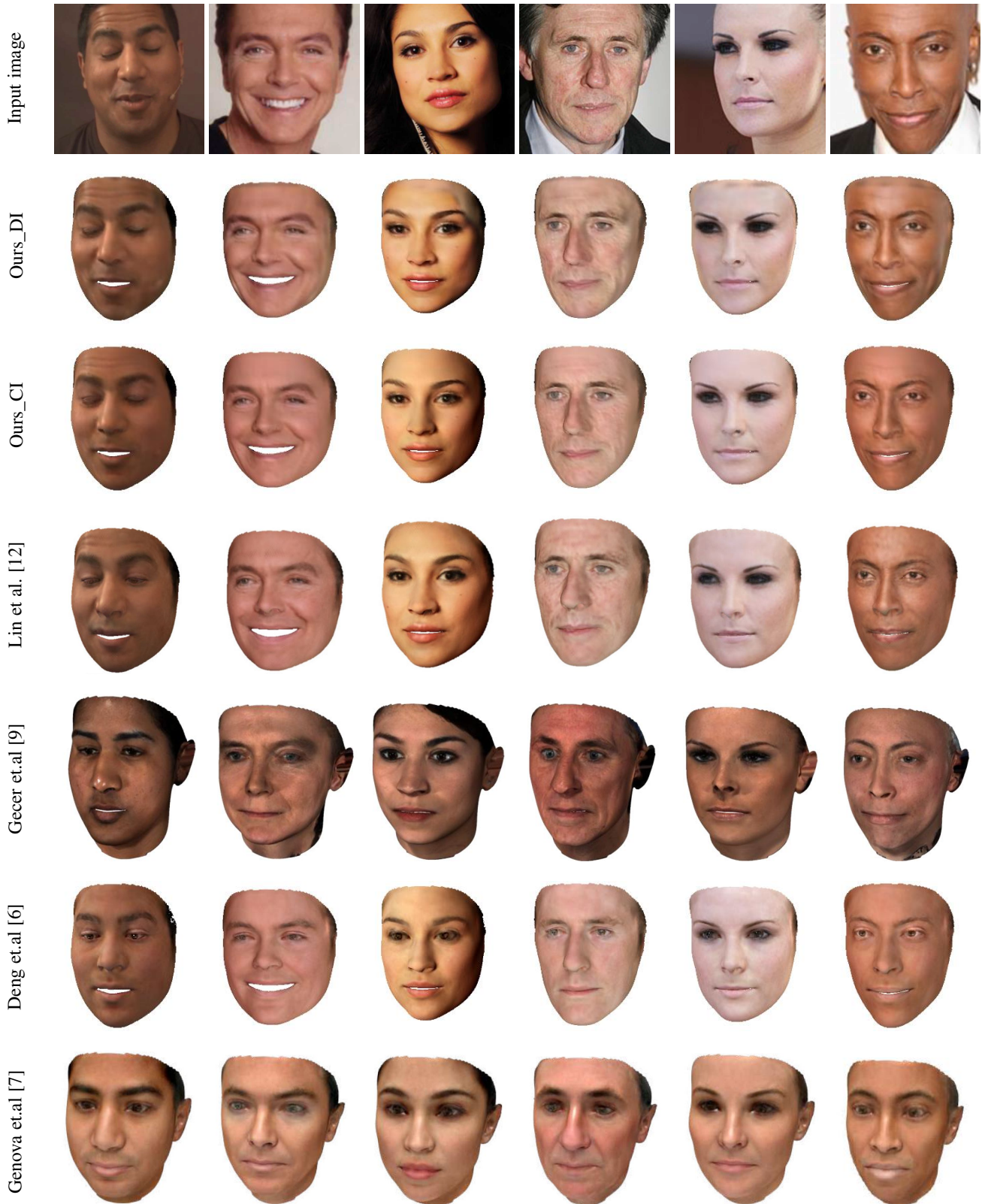
Fig. 8: **Qualitative comparison with other competitive methods.** The first row is the input images while the remaining rows show the reconstruction results of all methods. Our reconstructions are shown in the second and third rows where Ours_DI stands for reconstruction with detailed illumination and Ours_CI means reconstruction with coarse illumination.

Fig. 9: **Comparison of our results with Ganfit [9] in extreme lighting.** From left to right are input images, reconstructed albedo of [9], our generated albedo, and our re-illuminated results using a different illumination condition.

TABLE 3: **Quantitative comparison on CelebA dataset.** Ours_OD means the rendered image constructed by our detailed albedo combined with our detailed illumination, while Ours_OC means the rendered image constructed by our detailed albedo combined with coarse illumination. The best result of each measurement is marked in **bold** font. The symbol of '/' means that we could not test the corresponding method since no open-source implementation.

Methods	$L_1 \downarrow$	$PNSR \uparrow$	$SSIM \uparrow$	$LightCNN \uparrow$	$evoLVe \uparrow$
[6]	0.05	26.58	0.83	0.72	0.64
[9]	/	26.5	0.898	/	/
[12]	0.034	**29.69**	0.89	0.90	0.85
Ours_OC	0.02	24.88	0.89	0.91	0.83
Ours_OD	**0.01**	28.90	**0.93**	**0.93**	**0.86**

by using only detailed albedo combined with coarse illumination, which further demonstrates that our detailed albedo is able to capture most facial details in the input image.

5.4 Ablation Study

We conduct experiments to evaluate the influence of different components of our designed network.

Effectiveness of gradient and texture regularization losses. We first demonstrate the functionality of the gradient loss and texture regularization loss in our pipeline using the detailed rendering results with coarse illumination and detailed albedo. As shown in Fig. 10, our proposed L_{grad} helps our model to capture the detailed information from the facial image. Our $L_{tex-reg}$ loss contributes to the disentanglement of illumination and completes the occlusion part according to the prior albedo which renders the detailed albedo map more similar to the prior albedo map. By contrast, our full model produces the most convincing results than others.

illuminated results are rather realistic and keeps the identity information of the original image.

5.3 Quantitative Comparison

For quantitative comparison, we mainly focus on the criteria for measuring the image-level difference. First, L1 distance loss is applied as the basic pixel-level criterion. Then, we utilize two commonly-used image similarity criteria, namely the structural similarity index measure (SSIM) and peak signal-to-noise ratio (PSNR), to evaluate the similarity between the rendered face image and original input face image. With regard to the human face problem, we also leverage two well-known pre-trained face recognition networks as maps from image space to feature space and evaluate the difference between rendered face image and input face image in the facial feature space. The two facial recognition networks we adopted are *LightCNN* [59] and *evoLVe* [60], since their state-of-the-art performance and widely acceptance [12]. In summary, we calculate the difference between two face images in both pixel-level (including L1 distance loss, PSNR and SSIM) and face feature-level (including LightCNN and evoLVe).

The numerical statistics about these measurements for each method are reported in Table 3, where the competing methods we choose are state-of-the-art ones trying to reconstruct details in albedo. The table illustrates that our reconstruction results with detailed illumination are better than those of the competing algorithms. Besides, our framework also achieves competitive results

$Image$	$w/o\ L_{grad}$	$w/o\ L_{tex-reg}$	$Full\ model$

Fig. 10: **Ablation study of the proposed gradient loss and texture regularization loss:** our full model produces the most convincing results than others.

Effectiveness of light regularization. To evaluate the effect of our light perceptual regularization loss, we perform an ablation study by showing the rendered detailed illumination images with and without this loss. In Fig. 11, the light perceptual regularization loss helps the disentanglement of illumination with facial characteristics. The illumination map recovered with the help of light perceptual regularization loss includes less facial wrinkles and beard than the one that recovered without this loss. This phenomenon indicates that the facial details are all mostly
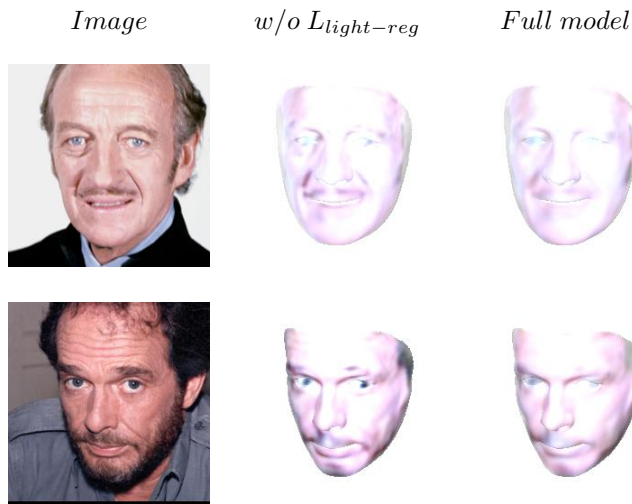
| Image | w/o $L_{light-reg}$ | Full model |

Fig. 11: **Ablation study of the proposed perceptual loss for lighting disentanglement:** the illumination image generated by our full model separates the facial intrinsic details better.

encoded in the detailed albedo map. Our illumination map has only environmental light information as far as possible thus, it is more suitable for re-renderable 3D facial generation.

5.5 Limitations

Although our model achieves competitive results on most of in-the-wild facial image datasets, it may still generate unreliable results on huge occlusion cases. The reason is that the prior model we used is only able to produce low-fidelity prior albedo and the lack of information in significantly occluded regions cannot be complemented with only symmetry regularization. Moreover, though our model takes 3DMM reconstructed albedo as prior, our reconstructed albedo is not completely independent of input image quality and generate better result when inputs are of high-resolution. Finally, the resolution of our uv map are only 256 and this limits the model's capability to adapt to high-resolution input images.

6 CONCLUSION AND FUTURE WORK

In this study, we present a novel self-supervised neural network for 3D face reconstruction, with an emphasis on generating re-renderable high-fidelity textures from single-view images. We utilize the coarse 3DMM model as a prior and fine-tune on it to capture more facial details, thus merging the advantages of generation-based and reconstruction-based methods. We compare our results with state-of-the-art methods in qualitative and quantitative ways. The comparison demonstrates that our method does not require capturing high-resolution face texture datasets and we can generate re-renderable and realistic facial textures.

In the future, we would first like to improve the generation model by constructing high-fidelity albedo map database and training a new generation model on it. This approach would significantly improve the fidelity. In addition, we are also interested in extending our model to reconstruct geometric details, because reconstruction of high-fidelity geometry and textures would lead to a more competitive and visually-appealing result. Finally, we wish to add more dynamics to our model and reconstruct animated facial details from a single image or video.

REFERENCES

[1] J. Thies, M. Zollhofer, M. Stamminger, C. Theobalt, and M. Nießner, "Face2face: Real-time face capture and reenactment of rgb videos," in *IEEE Computer Vision and Pattern Recognition (CVPR)*, 2016, pp. 2387–2395.

[2] A. Lattas, S. Moschoglou, B. Gecer, S. Ploumpis, V. Triantafyllou, A. Ghosh, and S. Zafeiriou, "Avatarme: Realistically renderable 3d facial reconstruction," in *IEEE Computer Vision and Pattern Recognition (CVPR)*, 2020, pp. 760–769.

[3] L. Hu, S. Saito, L. Wei, K. Nagano, J. Seo, J. Fursund, I. Sadeghi, C. Sun, Y.-C. Chen, and H. Li, "Avatar digitization from a single image for real-time rendering," *ACM Trans. on Graphics*, pp. 1–14, 2017.

[4] H. Zhou, J. Liu, Z. Liu, Y. Liu, and X. Wang, "Rotate-and-render: Unsupervised photorealistic face rotation from single-view images," in *IEEE Computer Vision and Pattern Recognition (CVPR)*, 2020, pp. 5911–5920.

[5] V. Blanz, T. Vetter, and A. Rockwood, "A morphable model for the synthesis of 3d faces," *ACM Trans. on Graphics (Proc. SIGGRAPH)*, pp. 187–194, 2002.

[6] Y. Deng, J. Yang, S. Xu, D. Chen, Y. Jia, and X. Tong, "Accurate 3d face reconstruction with weakly-supervised learning: From single image to image set," in *Proceedings of the IEEE Conference on Computer Vision and Pattern Recognition Workshops*, 2019, pp. 0–0.

[7] K. Genova, F. Cole, A. Maschinot, A. Sarna, D. Vlasic, and W. T. Freeman, "Unsupervised training for 3d morphable model regression," in *IEEE Computer Vision and Pattern Recognition (CVPR)*, 2018, pp. 8377–8386.

[8] A. Tewari, M. Zollhofer, H. Kim, P. Garrido, F. Bernard, P. Perez, and C. Theobalt, "Mofa: Model-based deep convolutional face autoencoder for unsupervised monocular reconstruction," in *Proceedings of the IEEE International Conference on Computer Vision Workshops*, 2017, pp. 1274–1283.

[9] B. Gecer, S. Ploumpis, I. Kotsia, and S. Zafeiriou, "Ganfit: Generative adversarial network fitting for high fidelity 3d face reconstruction," in *IEEE Computer Vision and Pattern Recognition (CVPR)*, 2019, pp. 1155–1164.

[10] L. Tran, F. Liu, and X. Liu, "Towards high-fidelity nonlinear 3d face morphable model," in *IEEE Computer Vision and Pattern Recognition (CVPR)*, 2019, pp. 1126–1135.

[11] L. Tran and X. Liu, "Nonlinear 3d face morphable model," in *IEEE Computer Vision and Pattern Recognition (CVPR)*, 2018, pp. 7346–7355.

[12] J. Lin, Y. Yuan, T. Shao, and K. Zhou, "Towards high-fidelity 3d face reconstruction from in-the-wild images using graph convolutional networks," in *IEEE Computer Vision and Pattern Recognition (CVPR)*, 2020, pp. 5891–5900.

[13] Y. Chen, F. Wu, Z. Wang, Y. Song, Y. Ling, and L. Bao, "Self-supervised learning of detailed 3d face reconstruction," *IEEE Trans. Image Process.*, pp. 8696–8705, 2020.

[14] A. Chen, Z. Chen, G. Zhang, K. Mitchell, and J. Yu, "Photo-realistic facial details synthesis from single image," in *IEEE International Conference on Computer Vision (ICCV)*, 2019, pp. 9429–9439.

[15] A. Tewari, F. Bernard, P. Garrido, G. Bharaj, M. Elgharib, H.-P. Seidel, P. Pérez, M. Zollhöfer, and C. Theobalt, "Fml: Face model learning from videos," *IEEE Computer Vision and Pattern Recognition (CVPR)*, pp. 10 812–10 822, 2019.

[16] A. Tewari, M. Zollhöfer, P. Garrido, F. Bernard, H. Kim, P. Pérez, and C. Theobalt, "Self-supervised multi-level face model learning for monocular reconstruction at over 250 hz," in *IEEE Computer Vision and Pattern Recognition (CVPR)*, 2018, pp. 2549–2559.

[17] A. S. Jackson, A. Bulat, V. Argyriou, and G. Tzimiropoulos, "Large pose 3d face reconstruction from a single image via direct volumetric cnn regression," in *IEEE International Conference on Computer Vision (ICCV)*, 2017, pp. 1031–1039.

[18] T. Karras, T. Aila, S. Laine, and J. Lehtinen, "Progressive growing of gans for improved quality, stability, and variation," *arXiv preprint arXiv:1710.10196*, 2017.

[19] J. Booth, A. Roussos, A. Ponniah, D. Dunaway, and S. Zafeiriou, "Large scale 3d morphable models," *Int. Journal of Computer Vision*, pp. 233–254, 2018.

[20] C. Cao, Y. Weng, S. Zhou, Y. Tong, and K. Zhou, "Facewarehouse: A 3d facial expression database for visual computing," *IEEE Trans. Vis. Comput. Graph*, pp. 413–425, 2013.

[21] T. Gerig, A. Forster, C. Blumer, B. Egger, M. Lüthi, S. Schönborn, and T. Vetter, "Morphable face models - an open framework," *2018 13th IEEE International Conference on Automatic Face & Gesture Recognition (FG 2018)*, pp. 75–82, 2018.

[22] P. Huber, G. Hu, R. J. Tena, P. Mortazavian, P. W. Koppen, J. W. Christmas, M. Rätsch, and J. Kittler, "A multiresolution 3d morphable face model and fitting framework," in *Proceedings of the 11th International Joint Conference on Computer Vision, Imaging and Computer Graphics Theory and Applications*, 2016, pp. 79–86.

[23] T. Li, T. Bolkart, J. M. Black, H. Li, and J. Romero, "Learning a model of facial shape and expression from 4d scans," *ACM Trans. on Graphics*, pp. 194:1–194:17, 2017.

[24] B. Egger, W. A. P. Smith, A. Tewari, S. Wuhrer, M. Zollhoefer, T. Beeler, F. Bernard, T. Bolkart, A. Kortylewski, S. Romdhani, C. Theobalt, V. Blanz, and T. Vetter, "3d morphable face models - past, present and future," *ACM Trans. on Graphics*, 2020.

[25] P. Paysan, R. Knothe, B. Amberg, S. Romdhani, and T. Vetter, "A 3d face model for pose and illumination invariant face recognition," *2009 Sixth IEEE International Conference on Advanced Video and Signal Based Surveillance*, pp. 296–301, 2009.

[26] V. Blanz and T. Vetter, "Face recognition based on fitting a 3d morphable model," *IEEE Trans. Pattern Anal. Mach. Intell.*, pp. 1063–1074, 2003.

[27] S. Romdhani and T. Vetter, "Estimating 3d shape and texture using pixel intensity, edges, specular highlights, texture constraints and a prior," *IEEE Computer Vision and Pattern Recognition (CVPR)*, pp. 986–993vol.2, 2005.

[28] D. M. Levine and C. Y. Yu, "State-of-the-art of 3d facial reconstruction methods for face recognition based on a single 2d training image per person," *Pattern Recognition Letters*, pp. 908–913, 2009.

[29] E. Richardson, M. Sela, and R. Kimmel, "3d face reconstruction by learning from synthetic data," *2016 Fourth International Conference on 3D Vision (3DV)*, pp. 460–469, 2016.

[30] E. Richardson, M. Sela, R. Or-El, and R. Kimmel, "Learning detailed face reconstruction from a single image," *IEEE Computer Vision and Pattern Recognition (CVPR)*, pp. 5553–5562, 2017.

[31] H. Yang, H. Zhu, Y. Wang, M. Huang, Q. Shen, R. Yang, and X. Cao, "Facescape: a large-scale high quality 3d face dataset and detailed riggable 3d face prediction," in *IEEE Computer Vision and Pattern Recognition (CVPR)*, 2020, pp. 601–610.

[32] K. Nagano, J. Seo, J. Xing, L. Wei, Z. Li, S. Saito, A. Agarwal, J. Fursund, and H. Li, "pagan: real-time avatars using dynamic textures," *ACM Trans. on Graphics*, pp. 1–12, 2018.

[33] S. Yamaguchi, S. Saito, K. Nagano, Y. Zhao, W. Chen, K. Olszewski, S. Morishima, and H. Li, "High-fidelity facial reflectance and geometry inference from an unconstrained image," *ACM Trans. on Graphics*, pp. 162:1–162:14, 2018.

[34] P. Garrido, M. Zollhöfer, D. Casas, L. Valgaerts, K. Varanasi, P. Perez, and C. Theobalt, "Reconstruction of personalized 3d face rigs from monocular video," *ACM Trans. on Graphics*, pp. 28:1–28:15, 2016.

[35] R. Zhang, P.-S. Tsai, J. E. Cryer, and M. Shah, "Shape from shading: A survey," *IEEE Trans. Pattern Anal. Mach. Intell.*, pp. 690–706, 1999.

[36] S. Wu, C. Rupprecht, and A. Vedaldi, "Unsupervised learning of probably symmetric deformable 3d objects from images in the wild," in *IEEE Computer Vision and Pattern Recognition (CVPR)*, 2020, pp. 1–10.

[37] G. Gafni, J. Thies, M. Zollhöfer, and M. Niessner, "Dynamic neural radiance fields for monocular 4d facial avatar reconstruction," in *IEEE Computer Vision and Pattern Recognition (CVPR)*, 2021.

[38] J. Thies, M. Zollhöfer, and M. Nießner, "Deferred neural rendering: image synthesis using neural textures," *ACM Trans. on Graphics*, pp. 1–12, 2019.

[39] H. Kim, P. Garrido, A. Tewari, W. Xu, J. Thies, M. Niessner, P. Pérez, C. Richardt, M. Zollhöfer, and C. Theobalt, "Deep video portraits," *ACM Trans. on Graphics*, pp. 1–14, 2018.

[40] J. Deng, S. Cheng, N. Xue, Y. Zhou, and S. Zafeiriou, "Uv-gan: Adversarial facial uv map completion for pose-invariant face recognition," *IEEE Computer Vision and Pattern Recognition (CVPR)*, pp. 7093–7102, 2018.

[41] C. Luo, J. Zhang, J. Yu, W. C. Chen, and S. Wang, "Real-time head pose estimation and face modeling from a depth image," *IEEE Trans. Multimedia*, pp. 2473–2481, 2019.

[42] X. Wang, Y. Guo, B. Deng, and J. Zhang, "Lightweight photometric stereo for facial details recovery," *IEEE Computer Vision and Pattern Recognition (CVPR)*, pp. 737–746, 2020.

[43] L. Zhang and D. Samaras, "Face recognition from a single training image under arbitrary unknown lighting using spherical harmonics," *IEEE Trans. Pattern Anal. Mach. Intell.*, pp. 351–363, 2006.

[44] T. Shi, Z. Zou, X. Song, Z. Song, C. Gu, C. Fan, and Y. Yuan, "Neutral face game character auto-creation via pokerface-gan," in *Proceedings of the 28th ACM International Conference on Multimedia*, 2020, pp. 3201–3209.

[45] W. Zhu, H. T. Wu, Z. Chen, N. Vesdapunt, and B. Wang, "Reda:reinforced differentiable attribute for 3d face reconstruction," in *IEEE Computer Vision and Pattern Recognition (CVPR)*, 2020, pp. 4958–4967.

[46] S. Liu, T. Li, W. Chen, and H. Li, "Soft rasterizer: A differentiable renderer for image-based 3d reasoning," *IEEE International Conference on Computer Vision (ICCV)*, pp. 7708–7717, 2019.

[47] H. Kato, Y. Ushiku, and T. Harada, "Neural 3d mesh renderer," in *IEEE Computer Vision and Pattern Recognition (CVPR)*, 2018, pp. 3907–3916.

[48] J. Deng, J. Guo, X. Niannan, and S. Zafeiriou, "Arcface: Additive angular margin loss for deep face recognition," in *IEEE Computer Vision and Pattern Recognition (CVPR)*, 2019, pp. 4690–4699.

[49] P. Isola, J.-Y. Zhu, T. Zhou, and A. A. Efros, "Image-to-image translation with conditional adversarial networks," *IEEE Computer Vision and Pattern Recognition (CVPR)*, pp. 1125–1134, 2017.

[50] C. Yu, J. Wang, C. Peng, C. Gao, G. Yu, and N. Sang, "Bisenet: Bilateral segmentation network for real-time semantic segmentation," *European Conference on Computer Vision (ECCV)*, pp. 325–341, 2018.

[51] Z. Liu, P. Luo, X. Wang, and X. Tang, "Deep learning face attributes in the wild," in *IEEE International Conference on Computer Vision (ICCV)*, 2015, pp. 3730–3738.

[52] Y. Feng, F. Wu, X. Shao, Y. Wang, and X. Zhou, "Joint 3d face reconstruction and dense alignment with position map regression network," in *European Conference on Computer Vision (ECCV)*, 2018, pp. 534–551.

[53] K. He, X. Zhang, S. Ren, and J. Sun, "Deep residual learning for image recognition," in *IEEE Computer Vision and Pattern Recognition (CVPR)*, 2016, pp. 770–778.

[54] X. Zhu, Z. Lei, X. Liu, H. Shi, and S. Z. Li, "Face alignment across large poses: A 3d solution," in *IEEE Computer Vision and Pattern Recognition (CVPR)*, 2016, pp. 146–155.

[55] D. Kingma and J. Ba, "Adam: A method for stochastic optimization," *International Conference on Learning Representations*, 2014.

[56] C.-H. Lee, Z. Liu, L. Wu, and P. Luo, "Maskgan: Towards diverse and interactive facial image manipulation," in *IEEE Computer Vision and Pattern Recognition (CVPR)*, 2020, pp. 5549–5558.

[57] F. Schroff, D. Kalenichenko, and J. Philbin, "Facenet: A unified embedding for face recognition and clustering," in *IEEE Computer Vision and Pattern Recognition (CVPR)*, 2015, pp. 815–823.

[58] A. Schneider, S. Schonborn, L. Frobeen, B. Egger, and T. Vetter, "Efficient global illumination for morphable models," in *IEEE International Conference on Computer Vision (ICCV)*, 2017, pp. 3865–3873.

[59] X. Wu, R. He, Z. Sun, and T. Tan, "A light cnn for deep face representation with noisy labels," *IEEE Transactions on Information Forensics and Security*, pp. 2884–2896, 2018.

[60] J. Zhao, J. Li, X. Tu, F. Zhao, Y. Xin, J. Xing, H. Liu, S. Yan, and J. Feng, "Multi-prototype networks for unconstrained set-based face recognition," in *IJCAI*, 2019.